Separation Science and Technology
Publication details, including instructions for authors and subscription information:
http://www.informaworld.com/smpp/title~content=t713708471

Effect of Pressure and Membrane Thickness on the Permeability of Gases in Dense Polyphenylene Oxide (PPO) Membranes: Thermodynamic Interpretation

Alsdeg Alsari[a]; Boguslaw Kruczek[a]; T. Matsuura[a]
[a] Department of Chemical Engineering, University of Ottawa, Ontario, Ottawa, Canada

To cite this Article Alsari, Alsdeg , Kruczek, Boguslaw and Matsuura, T.(2007) 'Effect of Pressure and Membrane Thickness on the Permeability of Gases in Dense Polyphenylene Oxide (PPO) Membranes: Thermodynamic Interpretation', Separation Science and Technology, 42: 10, 2143 — 2155
To link to this Article: DOI: 10.1080/01496390701446266
URL: http://dx.doi.org/10.1080/01496390701446266

Separation Science and Technology, 42: 2143–2155, 2007

ISSN 0149-6395 print/1520-5754 online
DOI: 10.1080/01496390701446266

Effect of Pressure and Membrane Thickness on the Permeability of Gases in Dense Polyphenylene Oxide (PPO) Membranes: Thermodynamic Interpretation

Alsdeg Alsari, Boguslaw Kruczek, and T. Matsuura
Department of Chemical Engineering, University of Ottawa, Ottawa, Ontario, Canada

Abstract: The permeability data of oxygen and nitrogen were obtained from both air and individual gas permeation experiments under different pressures using dense polyphenylene oxide (PPO) membranes of different thicknesses, after the membranes were fully stabilized. Opposite trends were observed with respect to oxygen and nitrogen as their permeabilities changed with changes in feed pressure and membrane thickness. Moreover, the pressure effect on oxygen permeability was reversed when the membrane was flipped upside down. Attempts were made to interpret the above experimental observations within a framework of entropy and enthalpy effect on the energy barrier for gas permeation and the change in the void space in the cross-sectional direction of a dense PPO membrane.

Keywords: Polyphenylene oxide, dense membrane, permeability, oxygen and nitrogen, pressure effect, thickness effort, effect of gas permeation direction

INTRODUCTION

Membrane gas separation emerged as an alternative gas separation technology almost three decades ago. Since then the research on gas separation membranes has concentrated in two major areas, development of new polymeric materials with very high intrinsic selectivities for gases, and

Received 7 September 2006, Accepted 2 February 2007
Address correspondence to Alsdeg Alsari, Department of Chemical Engineering, University of Ottawa, 161 Louis Pasteur, Ottawa, Ontario, Canada. Tel.: 1-613-562-5800 (x6114); Fax: 1-613-562-5172; E-mail: saddegalsari@yahoo.com

fabrication of defect-free, high productivity membranes. This research has led to some commercial applications of gas separation membranes including the production of high purity nitrogen from air, the recovery of hydrogen from mixtures with larger components such as nitrogen, methane, and carbon monoxide, and the purification of natural gas by removal of carbon dioxide (1).

Despite the fact that membranes have made many inroads in the field of gas separation, their market share in comparison with other competing technologies such as cryogenic distillation, absorption, and pressure swing adsorption is rather limited. Moreover, the number of commercial applications of gas separation membranes is quite low in comparison with the applications of reverse osmosis, ultrafiltration, and microfiltration membranes. One could use different arguments to explain this definite underachievement of membrane gas separations; however, it appears that one of the reasons is the difficulty in predictability of membrane permeability, which is caused by plasticization phenomena, aging, and sensitivity of the process to the defects on the membrane.

Permeability, P, of gas through a polymeric membrane is often related to the thermodynamic properties by the following equation,

$$P = DS = D_0 \exp\left[-\frac{E_D}{RT}\right] S_0 \exp\left[-\frac{\Delta H_s}{RT}\right] \tag{1}$$

where D and S are diffusion and solubility coefficient, respectively, E_D and H_s are the activation energy of diffusion (energy required to create a gap between polymer segments through which the gas molecules diffuse) and enthalpy of solution, respectively, and D_0 and S_0 are pre-exponential factors (2). R and T are universal gas constant and absolute temperature.

Looking into the diffusion coefficient more in detail, Singh and Koros further derived the equation for diffusional selectivity between gases A and B.

$$\frac{D_A}{D_B} = \exp\left[\frac{\Delta S^{\pm}_{A,B}}{R}\right] \exp\left[\frac{-\Delta E^{\pm}_{A,B}}{R}\right] \tag{2}$$

where $\Delta S^{\pm}_{A,B}$ and $\Delta E^{\pm}_{A,B}$ are differences of activation entropy and enthalpy, respectively, for the gases A and B. They have emphasized the importance of the entropic factor in the selectivity of the membranes made of zeolite and carbon molecular sieve (3). Using a similar relationship, Acharya and Foley evaluated the activation energies experimentally for nanoporous carbon membranes. The activation energies were further correlated to the molecular sizes of gases, assuming that the entropy term is dominant (4).

As for the membrane structure-performance relationship, it was reported that the selectivity of the top skin layer of the asymmetric membrane was higher than the dense membrane of the same polymeric material (5). Kawakami et al. further reported that the gas selectivity of asymmetric polyimide membranes with an ultrathin and defect-free surface thin layer increased with a decrease in the skin layer thickness. They attributed this

phenomenon to the formation of a better packed structure in a thinner skin layer, increasing density, and order in the molecular arrangement (6). Thus, the higher selectivity in the thinner polyimide membranes may have been caused by the decrease in entropy of gas molecules in the highly ordered macromolecular structure. Khulbe et al., on the other hand, studied the morphology of dense polyphenylene oxide (PPO) membranes by the combination of atomic force microscopy (AFM) and plasma etching technique and showed that the packing of nodules was the most compact at the top surface, the surface faced to air when the polymer dope was cast into a film, and the compactness diminished gradually as the distance from the top surface increased (7).

In this paper, the permeability data of oxygen and nitrogen were obtained from both air and individual gas permeation experiments under different pressures using dense polyphenylene oxide (PPO) membranes of different thicknesses, after the membranes were fully stabilized. Attempts were made to interpret the dependence of oxygen and nitrogen permeability on the feed gas pressure as well as the membrane thickness within a framework of the above-mentioned entropy and enthalpy effect on the energy barrier and the change in the macromolecular structure in the cross-sectional direction in a dense PPO membrane. This study will contribute to the better understanding of membrane gas permeation and particularly enable us to explain the peculiar behavior and poor reproducibility of permeation data obtained from the membranes even after they are stabilized.

EXPERIMENTAL

Membrane Preparation and Conditioning

Polyphenylene oxide (PPO, General Electric, T_g of 212°C and average molecular weight M_w of 40,000) was dried in a fume hood for at least 24 hrs. A 1 wt% solution of PPO in trichloroethylene (TCE from Aldrich) was prepared by dissolving the polymer under vigorous stirring for 24 hrs. The solution was filtered through a 1.2 μm Millipore filter and left for at least 24 hrs to remove air bubbles. Then, a certain amount of the filtered solution was poured into a stainless steel ring (diameter 7.2 cm) fixed on a precisely leveled glass plate. The amount of the solution allowed us to obtain the thickness of the membrane. The solution was left overnight, approximately 12 hours, for solvent evaporation, before the glass plate together with the cast solution film was immersed into a water bath until the membrane peeled off the glass plate spontaneously. The membranes were visually examined for defects such as dirt and pinholes. The membranes were further dried in ambient air for more than six hours, before being mounted to the permeation cells. The effective permeation area of the membrane was 13.2 cm^2. Unless otherwise stated, the air exposed side of the membrane, called top surface, when the polymer solution was poured into the metal ring, faced the feed gas stream.

Membrane stabilization was carried out by the following two methods before the permeation experiments for stabilized membranes were started.

1. Membranes, with thicknesses 6.7 and 10.6 μm, were subjected to continuous permeation experiments for two weeks using air at 25, 50, and 100 psig, respectively, until the permeation rate no longer changed. This confirms that the aging of the membranes was completed.
2. A membrane, with a thickness 12.4 μm was thermally dried at 100°C in a vacuum oven for 3 days and then air dried at ambient temperature. Our earlier study showed that the solvent was removed completely by this treatment.

The gas permeation experiments were carried out with air or pure oxygen and nitrogen under different pressures. The temperature was maintained at 22°C.

Automated Multi-cell Sweep-gas Constant Pressure System and Permeation Data Acquisition

The method used to measure the gas permeation rate is also known as the carrier gas method (8). It involves sweeping the permeated gas and routing it to be analysed for the fluxes of each penetrant. The technique employs a gas chromatograph (GC) as the selective detector for monitoring the variation in sweep gas mixture composition, as the gases permeate through the membrane.

The schematic of the experimental technique is shown in Fig. 1. The set-up is best described by categorizing it into five broad sections. Every section is interconnected and performs different functions at various stages of an

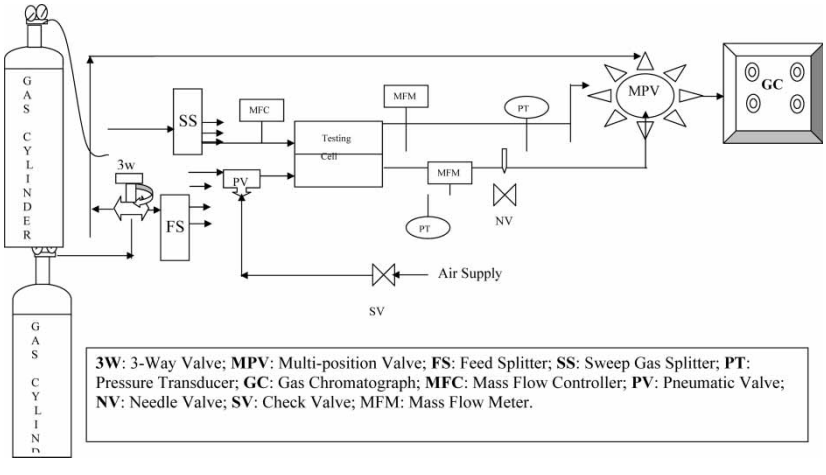

Figure 1. Schematic diagram of the sweep gas constant pressure (CP) system.

experimental run. Besides allowing mixed gas permeation experiments, the same set-up can be used for carrying out single gas permeation experiments, with minor modifications during data collection. For mixed gas permeation experiments, besides monitoring the gas flow rate, the concentration of the permeate gas mixture is also measured at regular time intervals. The present set-up employs in-line sampling technique for gas sample, followed by subsequent injection into a gas chromatograph for concentration analysis. The set-up is constructed with 316 stainless steel tubing and fittings for high pressure feed studies (0 to 500 psia). The entire set-up is automated for unsupervised operation by employing controller cards for the solenoid valve operation and data acquisition cards for pressure transducer and mass flow meter readings.

Feed Gas Supply and Regulatory System

The feed section supplies the test gases to the feed side of the membrane. The feed pressure is regulated by a two-stage pressure regulator and measured by a variable reluctance pressure transducer, from MKS, having a range 0–500 psia. The feed section is connected to the membrane cell through a 3-way valve. The feed side is connected to air-actuated pneumatic valves operated by solenoid valves to stop the feed to the cell in case of pressure increase, due to membrane rapture, in the permeate side.

Permeate and Retentate Sections

A sweep gas (methane) is fed to the permeate side of the cell to sweep the permeate gas out of the cell to the GC through a 9-position multi-port valve. A mass flow controller, from MKS, with a range of 0–10 cc/min, controls the sweep gas flow.

The gas permeation rate is monitored by mass flow meter (MFM) from MKS Instruments, having a range of $0–10 \pm 0.1$ cm^3/min. The pressure in the permeate side is monitored by a pressure transducer, from MKS Instruments, having a range of 0–50 psia. This is a safeguard against over-pressurization in the section due to membrane breakdown. A feedback closed loop control system monitors the opening and closing of the feed gas valve during an experimental run.

The retentate pressure is also measured by a pressure transducer, from MKS Instruments, having a range of 0–500 psia. The retentate flow rate is controlled by a needle valve (NV) and measured by a MFM similar to the one installed on the permeate side. This stage cut (gas permeation rate through the membrane/feed gas flow rate) is maintained to a low value by using the NV.

The sweep-permeate and retentate streams are connected to the multi position valve (MSV).

Gas Chromatograph In-line Sampling Interface

Series 580 TCD GC chromatograph, from GOW-MAC Instrument Co. was used for analyzing the gas streams coming from the feed and permeate gas lines. It contained two columns; one a porous polymer (Porapak) and the other a molecular sieve 5A. The detector was a thermal conductivity detector (TCD).

Data Acquisition and Control System

A switching controller module and a data acquisition controller board controlled the entire experimental system, including the gas chromatograph. The hardware was programmed using a graphical, user friendly, programmable software, LabVIEW 6.0, by National Instruments Inc. The program was capable of continuously recording and storing pressures (both upstream and downstream), flow rates (sweep gas, permeate, and retentate), and the temperature at the permeation cell. The process control includes the operation of the valves and mass flow controllers according to the preset parameters such as up-stream and down-stream pressures, temperature, sweep flow rate, and the status of the valves. The system also controlled the GC operation such as the switching between injecting and purging, and between series and by-pass positions. It also recorded data from the GC, and calculated areas of peaks that represented the analyzed gases. From this system the permeation rate for each permeant, Q_i, can be obtained from the gas flow rate on the permeate side and the permeate gas composition.

Data Processing

The permeability (Barrer $= 10^{-10}$ cm^3 (STP) cm/cm^2 s cmHg), P_i, for oxygen and nitrogen can be calculated by

$$P_i = Q_i l / \Delta p_i A \times 10^{10} \tag{3}$$

where, Q_i and Δp_i are the permeation rate (cm^3 (STP)/s) and the cross-membrane partial pressure difference of component i (either oxygen or nitrogen, cmHg), respectively, A is the effective area for permeation of the membrane (cm^2) and l is the membrane thickness (cm).

The permeability ratio, is obtained by

$$\alpha = (P_{oxygen})/(P_{nitrogen}) \tag{4}$$

It should be noted that the above equations are applicable for both single gas (either oxygen or nitrogen) and mixed gas (air in the feed) experiments.

RESULTS

Figure 2 shows the results of air permeation experiments. The permeability of O_2 and N_2 is shown for membranes of different thicknesses at different feed air pressures. O_2 permeability increases with an increase in pressure continuously from 25 to 100 psig (1 psi = 6889 Pa). On the other hand, O_2 permeability decreases with an increase in membrane thickness. N_2 permeability decreases from 25 to 50 psig, and shows little change from 50 to 100 psig. N_2 permeability increases with an increase in membrane thickness from 6.7 to 10.6 μm and then levels off with a further increase in the thickness. Figure 3 shows that the permeability ratio generally increases with the feed pressure. For 12.4 μm membrane, the permeability ratio decreases only slightly when the pressure is increased from 50 to 100 psig. It is also

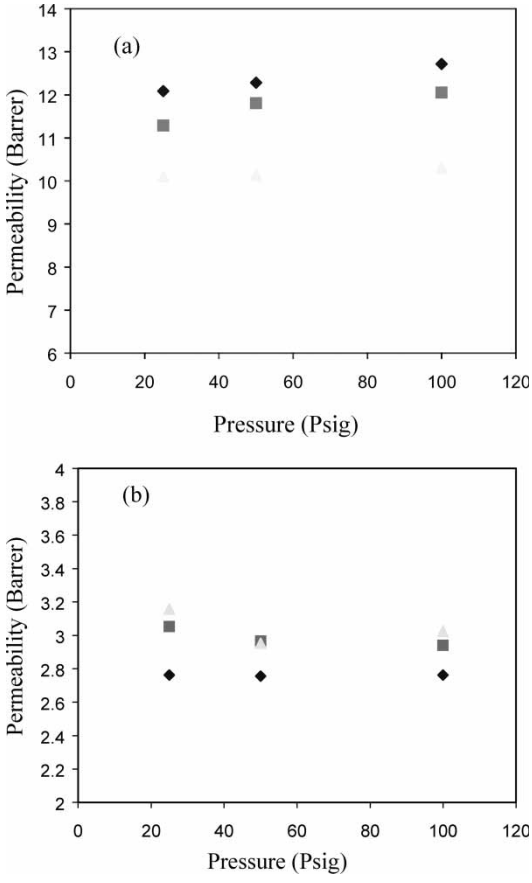

Figure 2. Permeability change with air pressure (a) O_2 (b) N_2 of membranes with different thickness ◆ 6.7 μm, ■ 10.6 μ m and ▲ 12.4 μm.

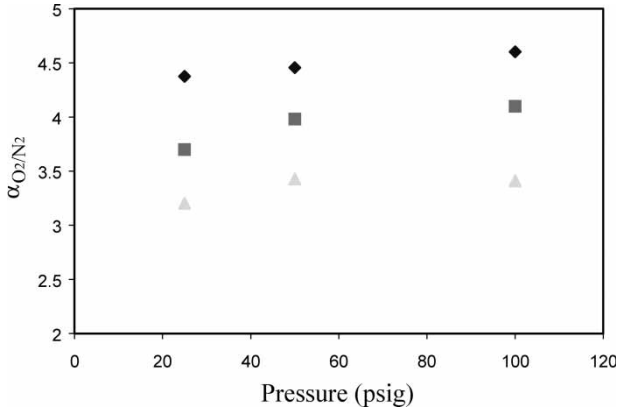

Figure 3. Permeability ratio $\alpha_{O2/N2}$ change with air feed pressure for membranes with different thickness ◆ 6.7 μm, ■ 10.6 μm and ▲ 12.4 μm.

observed that the permeability ratio decreases with an increase in the membrane thickness. Nearly the same trends in the O_2 permeability and N_2 permeability that were observed for the three different membranes ensure that the membranes were equally stabilized regardless of the adopted stabilizing procedures. The permeability data shown in Fig. 2 are lower than those obtained in the previous work (7) because in the present work the permeability data were obtained after a much longer period of aging.

Figure 4 shows experimental results for the permeation of single gases, when the membrane thickness was 12.4 μm. Generally, higher permeability values were obtained from the air experiments than the single gas experiments for both oxygen and nitrogen, although the trend observed for the effect of the

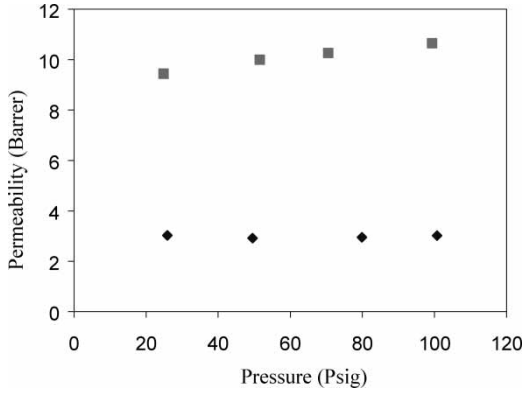

Figure 4. Change of permeability of single gases permeation ■ O_2 and ◆ N_2 for 12.4 μm.

pressure on the oxygen and nitrogen permeability was the same for both air and single gas experiments. Differences in the permeability values between the air experiments and the single gas experiments suggest that the presence of one gas affects the permeability of the other.

The symmetry test was conducted by a set of experiments using a membrane with a thickness of 8.3 μm. The membrane was subjected to a stabilization procedure similar to the membranes with thicknesses 6.7 and 10.6 μm. Here, the definition of the membrane surface is in order. The surface which was exposed to air, when the polymer solution was cast, is called "top side," while the surface that was in contact with the glass plate is called the "bottom side." The top side was always in contact with the air stream during the permeation and separation experiments, unless otherwise stated. In the symmetry test, pressure was changed progressively from 100 to 50 and then to 25 psig within the first 15 hours, maintained at 25 psig for 13 hours and then brought back to 100 psig during the last 17 hours. This pressure change is illustrated in Fig. 5. Then, the membrane was flipped upside down; i.e., the bottom side was brought into contact with the feed air stream. The same program for the pressure change was applied. The permeability data are also shown in Fig. 5. The following trends are observed from the figure.

1. The permeability of both oxygen and nitrogen decreased when the direction of the air permeation was changed.
2. For nitrogen gas, the permeability decreased as the pressure increased regardless of the air permeation direction. This trend is the same as that shown in Fig. 2.
3. For oxygen gas, the permeability increased as the pressure increased when the direction of air permeation was from the top to the bottom side. This trend is the same as those given in Figs. 2 and 4.
4. The oxygen permeability, however, decreased as the pressure increased when the direction of the air flow was reversed.

In other words, the performance of the membrane was not symmetric across the cross-section.

DISCUSSION

The experimental data presented in Figs. 2–5 can be explained within the framework of the following assumptions.

1. As the pressure increases, the macromolecular segments are displaced close to each other. As a result of this segmental motion, the inter-segmental void space decreases and the density of the polymer increases. This segmental motion is reversible.

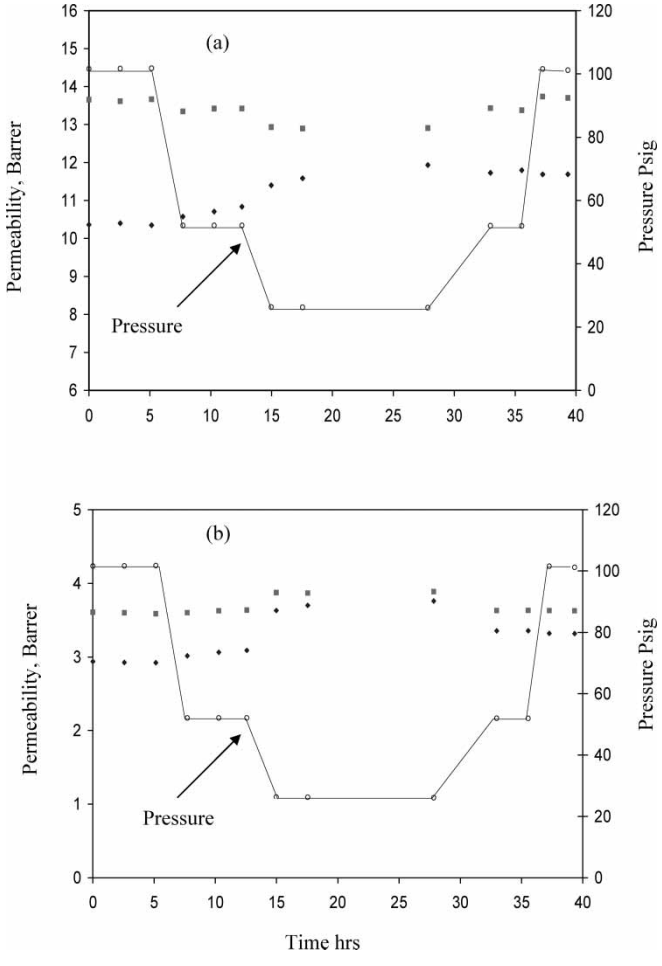

Figure 5. Permeability change with air pressure (a) O_2 (b) N_2 for membranes fed from different surfaces ■ top surface, ▲ bottom surface.

2. The energy barrier to be overcome for the transport of gas molecules through the membrane is closely related to the molar Gibbs free energy of gas molecules in the void space. In the presence of affinity forces between the gas molecule and the macromolecular segment, the enthalpy of the gas decreases with a decrease in the void volume since more gas molecules will be under the influence of the affinity forces. The Gibbs free energy, as well as the energy barrier for the transport, decreases ($\Delta G = \Delta H - T\Delta S$), leading to higher permeability. With a further decrease in the void volume, the entropy of the gas molecules starts to decrease, since the gas molecules are packed in a more ordered form in the smaller void space. Then, the Gibbs free energy increases,

leading to lower permeability. In the absence of affinity forces between the gas molecule and the macromolecular segment, on the other hand, the enthalpy effect can be ignored. In this case, gas permeability decreases monotonically as the void space decreases. The effect of void space decrease on the permeability is schematically presented in Fig. 6a (in the presence of affinity forces) and b (in the absence of the affinity forces).

Oxygen molecules are more attracted to the macromolecular segment of PPO than nitrogen molecules. This is evidenced by the higher solubility of oxygen in PPO (9, 10). Therefore the permeability pattern given in Fig. 6a is applicable for oxygen, while pattern Fig. 6b for nitrogen.

3. Even though dense PPO membranes were prepared in this work, they have morphological asymmetry. The polymer density is the function of the distance from the top surface. As the distance increases, the density decreases.

With the three assumptions stated above, the experimental results given in Fig. 2a and 2b can be explained. In the case of oxygen, the inter-segmental void space decreases and gas permeability increases with an increase in the total gas pressure, particularly when gas molecules are in the region governed by enthalpy. (Region A in Fig. 6a). As the membrane thickness increases, the overall density of the membrane decreases, therefore the gas permeability decreases. In the case of nitrogen, on the other hand, the enthalpy dominant region does not exist (Fig. 6b). As a result, nitrogen permeability decreases with an increase in pressure and increases with an increase in membrane thickness. Figure 3 is simply a result of the combination of Figs. 2a and 2b. Figure 4 confirms the trend observed in air experiments by the experiments with individual gases.

The results shown in Fig. 5 can be explained considering the pressure distribution across the membrane is from high to low as you go down from the feed side to the permeate side. When the membrane is flipped upside down, the lower density side of the membrane is near the feed gas and compacted more under higher pressure (Fig. 7b). Before flipping the membrane, the high density side of the membrane was near the feed gas

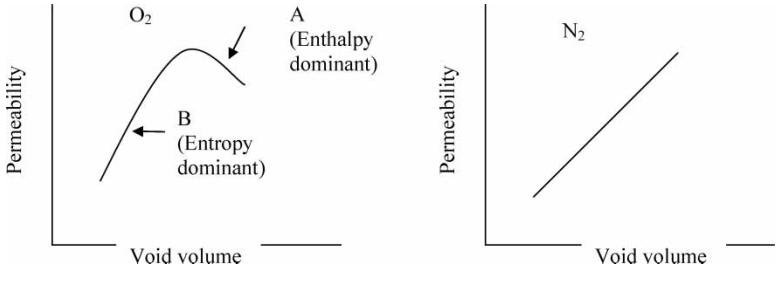

Figure 6. Permeability change with void volume: schematic illustration (a) oxygen, (b) nitrogen.

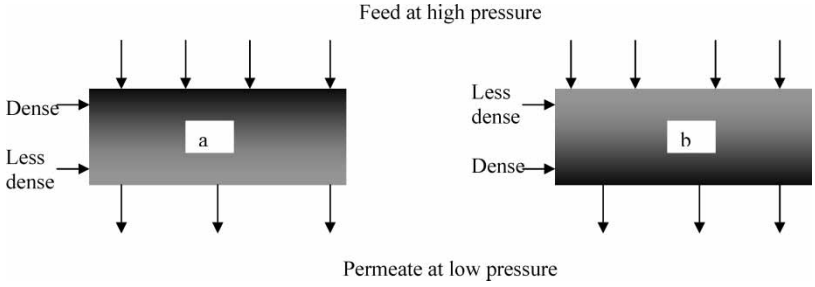

Figure 7. Membrane surfaces facing feed air (a) top surface is in contact with feed air, (b) bottom surface is in contact with air.

(Fig. 7a) and compaction was not as effective as after membrane flipping. Therefore, the overall density of the membrane becomes higher after membrane flipping. This increase in density brings the membrane to the entropy governing region (Region B in Fig. 6a) of the oxygen permeation. The membrane with a small thickness, 8.3 μm was used in this experiment. Since this membrane had already quite a high density due to its thinness, a further increase in density may bring the permeability into the entropy dominate region. Hence, the oxygen permeability decreases as the pressure increases. The oxygen permeability is also lower after membrane flipping than before flipping.

Nitrogen permeability on the other hand, always decreases as the pressure increases according to Fig. 6a. It also decreases when the membrane is flipped.

CONCLUSION

Conclusions drawn from this investigation:

The effect of feed gas pressure and membrane thickness on the permeability of oxygen and nitrogen gas has been evaluated. They are characterized by the decrease in the volume of the void space where the gas permeation takes place, the change in the entropy and enthalpy of gas molecules with the change in the void volume as well as the asymmetric structure of the dense PPO membranes. The dependence of the feed gas pressure effect on the direction of gas permeation can also be explained.

REFERENCES

1. Prasad, R., Shaner, R.L., and Doshi, K.J. (1994) Comparison of membranes with other gas separation technologies. In *Polymer Gas Separation Membranes*; Paul, D.R. and Yampol'skii, Yu. (eds.); CRC Press: London, U.K.

2. Vieth, R.W. (1991) *Diffusion in and Through Polymers*; Carl Hanser: Munich, Germany, Chap. 4.
3. Singh, A. and Koros, W.J. (1996) Significance of entropic selectivity for advanced gas separation. *Ind. Eng. Chem. Res.*, 35: 1231–1234.
4. Acharya, M. and Foley, H.C. (2000) Transport in nanoporous carbon membranes: experiments and analysis. *A.I.Ch.E J.*, 46: 911–921.
5. Pfromm, P.H., Pinnau, I., and Koros, W.J. (1993) Gas transport through integral-asymmetric membranes: a comparison to isotropic film transport properties. *J. Appl. Polym. Sci.*, 48: 2161–2171.
6. Kawakami, H., Mikawa, M., and Nagaoka, S. (1998) Gas transport properties of asymmetric polyimide membrane with an ultrathin surface skin layer. *Macromolecules*, 31: 6636–6638.
7. Khulbe, K.C., Matsuura, T., and Noh, S.H. (1998) Effect of thickness of the PPO membranes on the surface morphology. *J. Memb. Sci.*, 145: 243–251.
8. Koros, W.J. and Chern, R.T. (1989) Separation of gaseous mixtures using polymer membranes. *Handbook of Separation Process Technology*Rousseau, R.W. (ed.); Wiley: New York.
9. Capitani, D., Clericuzio, M., Fiordiponti, P., Lillo, F., and Segre, A.L. (1993) Oxygen adsorption on poly (2′6-dimethyl) phenyleneoxide. A solid state H-NMR study. *Eur. Polym. J.*, 29: 1451–1456.
10. Alentiev, A., Drioli, E., Gokzhaev, M., Golemme, G., Ilinich, O., Lapkin, A., Volkov, V., and Yampolskii, Yu. (1998) Gas permeation properties of phenylene oxide polymers. *J. Membr. Sci.*, 138: 99–107.